Applied Thermal Engineering 148 (2019) 674–683

Contents lists available at ScienceDirect

Applied Thermal Engineering

journal homepage: www.elsevier.com/locate/apthermeng

Research Paper

Numerical simulations for evaluating the impact of advanced insulation coatings on H_2 additivated gasoline lean combustion in a turbocharged spark-ignited engine

A. Broatch, P. Olmeda, X. Margot, J. Gomez-Soriano*

CMT – Motores Térmicos, Universitat Politècnica de València, Camino de Vera, 46022 Valencia, Spain

HIGHLIGHTS

- The effect of surface roughness has been assessed in a spark-ignited engine.
- Some effect of the surface roughness on the combustion has been observed.
- In general, the combustion rate is reduced as the roughness is increased.
- The gain in HT with smart coatings is very limited while the knock tendency rises.

ARTICLE INFO

Keywords:
Spark-ignited engine
CFD modelling
Insulation coatings
Heat transfer
Knock

ABSTRACT

This paper presents a numerical methodology based on Computational Fluid Dynamics (CFD) simulations to understand the physics of heat losses through the cylinder walls coated with different materials, taking into account other important factors such as surface roughness and near wall flow velocity in a turbocharged spark-ignited (SI) engine. Engine closed cycle simulations have been performed to estimate the thermodynamic evolution of the charge inside the cylinder and therefore, to evaluate the effect of roughness on heat transfer and combustion at real operating conditions. The model has been validated by using experimental data for two different steady-state operation conditions of a fully instrumented engine. In general, the maximum rate of heat release is reduced as the roughness is increased. Observed trends indicate that the heat transfer variation is mainly caused by changes in the combustion process due to the surface roughness, rather than to the effects of the coating material properties/characteristics (the increase of the effective contact area, porosity, etc.). Lastly, the comparison between uncoated and coated engine have shown that maximal gains around 5% in heat loss could be achieved, with very limited efficiency improvement, whereas the knock tendency increases.

1. Introduction

Spark-ignited (SI) engines are becoming the focus of current research in internal combustion engines (ICE). In view of the current socio-political restrictions and market demands, automotive manufacturers are allocating a large amount of resources in R&D to further develop SI engines. Specifically, in terms of their efficiency, since they are still one step behind Diesel engines.

As happened with Diesel engines a couple of decades ago, strategies such as turbocharging, the increase of the compression ratio or exhaust gases dilution are being applied in order to improve the power engine output, while reducing greenhouse gas emissions (CO_2) of modern SI engines. Although these strategies allow a certain degree of improvement, the new enhanced thermodynamic conditions inside the chamber lead to an increase in knock propensity [1], thus compromising the engine reliability and durability.

Despite many in depth studies over the last years [2], knocking combustion still appears to be the main bottleneck that prevents achieving higher thermal efficiency in SI engines. Other solutions, namely the Miller cycle or stratified charge mixtures, have shown clear advantages for reducing knocking [3,4]. The Miller cycle, for example, aims at reducing the effective compression ratio by means of an early intake valve closing (IVC) without causing excessive efficiency losses. This method allows to minimizing pumping losses at low loads whereas the gross indicated efficiency is deteriorated due to the lack of turbulence that compromises the burning rate [5]. The charge stratification,

* Corresponding author.
E-mail address: jogoso1@mot.upv.es (J. Gomez-Soriano).

https://doi.org/10.1016/j.applthermaleng.2018.11.106
Received 31 August 2018; Received in revised form 22 November 2018; Accepted 24 November 2018
Available online 24 November 2018
1359-4311/

on the other hand, allows keeping —or even improving— efficiency levels while controlling the knock appearance by enhancing the burning velocity at the spark plug location. However, an increased cycle-to-cycle variability (CCV) was observed in several studies due to the complexity of reproducing the exact local mixture properties between two consecutive cycles [6].

Most recent studies focus on decreasing the air-fuel ratio by minimizing the fuel amount at every engine cycle. Operating under these lean conditions allows at least *a priori* increasing the thermal efficiency when burning rates remain comparable to those achieved in stoichiometric conditions. Nonetheless, excessive diluted blends near the spark plug increase the number of misfiring cycles, while conditioning the burning rate drastically and therefore raising the CCV [7].

In this situation, the use of additives to enhance the burning velocity and stability appears as a promising path worth exploring [8]. For instance, the addition of hydrogen (H_2), which is produced *in situ* onboard the vehicle by electrolysis of water, has been shown to be an alternative to improve engine performance, due to its faster and cleaner burning characteristics [9,10].

Furthermore, reducing the heat transfer (HT) through the chamber walls is still a hot topic today [11–13]. Although the use of ceramic insulation coatings brings about a notable HT decrease that may lead to an improved cycle efficiency, the negative HT flow –heat from walls to gas– heats up the intake fresh gases during the exchange process. This results in a significant deterioration of the volumetric efficiency that in turn conditions the efficiency levels [14]. Nevertheless, some authors [15,16] claim that "smart" insulation coatings – smart understood as a particular configuration of both material and geometric features– imitate the temperature swing along the engine cycle, thereby reducing thermal losses during the combustion, while keeping the surface temperature low enough to maintain the volumetric efficiency [17].

Toyota Central R&D Labs Inc. conducted relevant investigations on this topic considering both SI and Diesel engines [16–19]. In all these works, they show that materials with low conductivity and thermal capacitance applied to the piston surface can help to reduce HT during combustion, thereby improving thermal efficiency. However, multiple discrepancies among the papers question the validity of their conclusions. In particular, it has been demonstrated that the technique used for measuring the surface temperature —Laser-Induced Phosphoresce [20]— systematically overestimates traditional thermocouple measurements and simulation results [21]. In addition, some of the conclusions of *Toyota's* papers disagree with most of the investigations carried out to date. From Heywoods's classical work [22] to more recent studies performed by Rakopoulos, Chang, Kikusato et al. [23–25], the maximum temperature swing, and thus the gain in HT, is significantly lower than the values published by *Toyota*.

In view of these contradictory discussions, the main objective of this paper is to assess the suitability of advanced coating insulations of in-cylinder parts to reduce the heat losses and to quantify the impact of this technology on the indicated efficiency of a turbocharged SI engine operating under lean conditions with H_2 additive. In order to achieve this target a computational methodology for the evaluation of the heat losses in the combustion system with coating insulation has been developed to further understand the physics of heat losses through the cylinder walls coated with different materials, taking into account other important factors such as surface roughness and near wall flow velocity.

In the following sections of this paper, the methodology, its validation and the obtained results are presented. In Section 2, the methodology followed in this research work is described in detail. Section 3 is dedicated to the validation of the previous methodology considering two real engine operating conditions and paying special attention to the kinetic mechanism features (ignition delay and laminar flame speed). Section 4 discusses the results obtained with the outlined method by varying the wall roughness for both an uncoated engine with a standard aluminium block and a coated one. Finally, Section 5 summarizes the main conclusions drawn from this study.

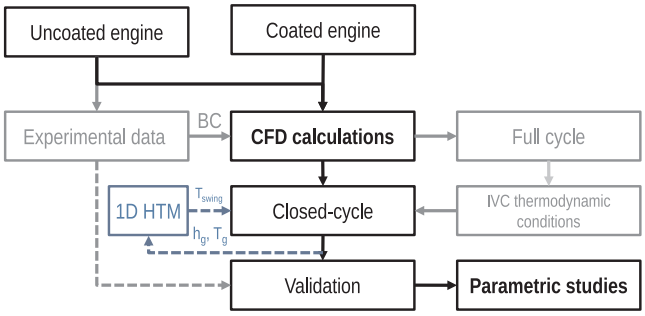

Fig. 1. Chain of 3D simulations to evaluate the impact of the roughness and coating.

2. Methodology

A new methodology has been defined on the basis of a Computational Fluid Dynamics (CFD) model. This is schematically summarized in Fig. 1 in order to clarify the modelling approach and the link between the various simulation steps.

First, the gas exchange process (GEP) is simulated using a calculation domain that includes the complete cylinder, as well as the intake and exhaust ports. The GEP starts at exhaust valve opening (EVO) with zero velocity and uniformly-distributed initial conditions of pressure, temperature, turbulence and species concentration across the whole domain.

Once the GEP has been calculated, closed cycle simulations may be performed starting from the resulting flow conditions at IVC.

For the closed cycle simulations two different engine configurations are used: the conventional uncoated engine (without coating insulation) and a modified engine with a coating layer in both piston and cylinder head surfaces. Both configurations are based on the reference engine configuration described in Table 1. The coating layer has 100 μm thickness and is formed of a material characterized by a conductivity (k) of 1.5 W $m^{-1}K^{-1}$ and a thermal capacitance of (ρc) 3500 kJ $m^{-3}K^{-1}$. The calculations are performed for both engine configurations at two real operation conditions defined in Table 2, and taking into account three levels of coated surface roughness, in addition to the smooth surface case. Therefore, the combination of all variations, operating points and surface features, has resulted in 16 simulations summarized in the same Table 2. In all these tests, the quantity of H_2 is expressed in volumetric fraction with respect to the air flow rate at the intake manifold.

Since the impact of negative heat loss (due to the wall to gas heating) on volumetric efficiency is not significant according to conclusions drawn from a preliminary analysis using 0D/1D modelling with the aforementioned coating material, in this study the initial conditions at IVC have been considered equal in all cases. Consequently, this study supposes that the negative heat transfer during the intake stroke is equal in both engine configurations.

In both engine configurations, a surface temperature swing caused by the cyclic intermittency of combustion has been imposed as boundary condition on the piston and cylinder head, since this is one of the most interesting features obtained with this kind of insulation materials. The temperature swing has been calculated with a 1D HTM

Table 1
Main specifications of the engine.

Engine type	SI engine
Number of cylinders [–]	1
Bore [mm]	75.0
Stroke [mm]	93.0
Compression ratio [–]	14:1
Number of valves [–]	2 intake and 2 exhaust

Table 2
Values of the main parameters used in each of the sixteen numerical simulations.

Operating point	#1		#2	
Configuration	Uncoated	Coated	Uncoated	Coated
Engine speed [rpm]	2500		3000	
IMEP [bar]	9		13	
Intake pressure [bar]	1.465		2.032	
Spark advance [cad aTDC]	−20.0		−21.5	
Start of injection [cad aTDC]	−290.0		-290.0	
λ [–]	2		2	
H_2 [%]	4		3	
R_a (surface roughness) [μm]	0,6,14,40		0,6,14,40	

(Heat Transfer Model) described later, using as input variables the gas conditions (temperature and convective heat transfer coefficient) calculated by means of CFD. Fig. 1 shows a schematic view of the connection between the 1D and 3D calculations. The calculations with combustion performed for the smooth uncoated engine points yielded new gas temperature and convective heat transfer coefficient profiles, which were used to calculate again the temperature swing and compare it with the previous one. Results indicated less than 1.4 K of maximum difference between both profiles after the first iteration, thereby confirming the good estimation of the wall temperatures.

The model has been validated by comparing the in-cylinder pressure trace measured at IFP Energies nouvelles (IFPEN) laboratories for the uncoated engine in the two operation conditions displayed in Table 2. Prior to the model validation, the kinetic mechanism of the utilized surrogate has been validated in terms of flame speed and auto-ignition delay with experimental data available in the literature.

Finally, the evaluation of the impact of coating roughness has been performed through the analysis of the Rate of Heat Release (RoHR), several thermodynamic in-cylinder conditions, the heat transfer across the chamber walls, the knock tendency and both combustion and indicated efficiencies.

2.1. CFD model set-up

This section describes the numerical model used to analyze the impact of the surface roughness on the combustion process. Key aspects of the virtual model, specifically those related to the combustion and spark ignition simulation, are detailed.

The engine calculations performed in this research have been performed with the commercial CFD code CONVERGE v2.3 [26], which is based on the finite-volume method. A second-order central difference scheme has been used for spatial discretization and a first-order scheme for temporal discretization.

In-cylinder turbulence was modelled using the Unsteady Reynolds-Averaged Navier Stokes (URANS) based re-normalized group (RNG) k-ϵ model [27] coupled with the wall heat transfer model developed by O'Rourke and Amsden [28]. The Redlich-Kwong equation [29] was selected as the equation of state for calculating the compressible flow properties. Pressure-velocity coupling was achieved by using a modified Pressure Implicit with Splitting of Operators (PISO) method [30].

The computational domain shown in Fig. 2 was created from the real engine geometry provided by IFPEN and it includes the complete single cylinder geometry and the intake/exhaust ports for full cycle calculations. The cut-cell Cartesian method available in the code was used to generate a hexahedral mesh with a base size of 2 mm. The cell size was reduced to 0.5 mm at the walls of the combustion chamber ports and valves regions to improve boundary layer prediction. Moreover, the mesh size in the chamber was decreased to 1 mm, and in the region of the spark plug to 0.125 mm to resolve both the spark and the developing primary flame kernel. An adaptive mesh refinement (AMR) was also activated to increase grid resolution (up to 0.5 mm minimum cell size) based on the velocity and temperature sub-grid scales of 1 ms^{-1} and 2.5 K, respectively. Previous RANS [31–33] and large eddy simulations (LES) studies [34,35] have demonstrated that this mesh configuration is sufficient for simulating the flame propagation and knocking combustion in SI combustion. The peak cell count in the simulations reached 1.5 million approximately.

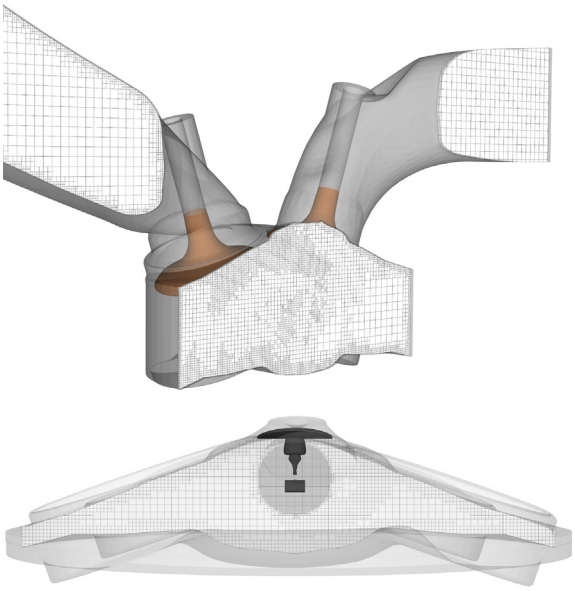

Fig. 2. A schematic of the computational domain and mesh characteristics, including intake and exhaust pipes/valves and combustion chamber.

For combustion modelling, the SAGE detailed chemistry solver [36] was employed along with a multi-zone (MZ) approach, with bins of 5 K in temperature and 0.05 in equivalence ratio [37]. Although it does not use an explicit turbulent combustion closure [38,39], it has been demonstrated in previous studies [40] that the SAGE-MZ model performs well for simulations of lean gasoline combustion in the context of RANS. The chemical mechanism was based on a Primary Reference Fuel (PRF) of iso-octane and an adapted reaction mechanism with 73 species and 296 reactions specifically developed for SI engine simulations [41]. The incipient spark kernel was modelled by adding a volumetric source for the energy equation, a sphere of radius 0.5 mm in the spark gap at spark timing. The amount of energy transferred to the fluid was fixed as 60 mJ uniformly distributed along a L-type profile [42].

Wall temperatures were assumed to be constant and estimated by 1D modelling for the GEP simulation [43]. Instantaneous temperature and pressure measurements at intake/exhaust manifolds were used as inflow/outflow boundaries placed at the end of the intake and exhaust ports. Subsequently, the thermodynamic conditions obtained from the GEP simulation were considered as initialization values for the closed cycle calculations. In this case, the temperature swing of the chamber walls was considered and it was calculated linking the CFD model with the 1D heat transfer model explained below. As example, the temperature swings considered for both engine configurations at the operating Point #2 are shown in Fig. 3.

Finally, the effect of the surface roughness was simulated by modifying the law-of-the-wall according to Cebeci & Cousteix [44] who proposed a mean velocity modified by a roughness length parameter (R_a) to account for the shift of the intercept due to roughness effects.

2.2. 1D heat transfer model

This section briefly describes the theoretical background used as basis to evaluate the heat losses when adding an insulation on the internal walls of the combustion chamber.

As in the theoretical problem proposed by Bejan and Kraus [45],

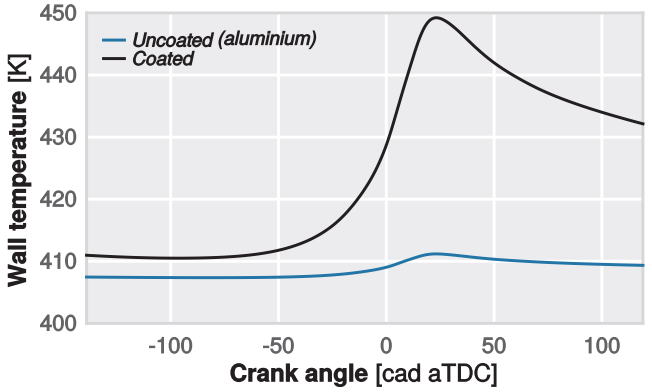

Fig. 3. Temperature swing profiles for 3000 rpm - 13 bar cases using aluminium and 100 μm of coating material.

some hypotheses are made in order to solve the instantaneous heat transfer through the solid surfaces of the combustion chamber.

- The calculation domain is a semi-infinite solid; the heat transfer flow is one-dimensional.
- The solid consists of one material with constant properties (*k, ρ and c*).
- The heat transfer coefficient between the gas and the solid surface is constant.

Taking into account these hypotheses, the boundary condition on the gas side of the solid surface is

$$\dot{q} = h(T_g - T_s) = -k\frac{\partial T}{\partial x}\bigg|_{x=0} \quad (1)$$

where T_s represents the solid temperature at the interface and T is the solid temperature at any point of the solid.

And the unsteady one-dimensional heat conduction equation is solved in the semi-infinite solid by

$$\frac{\partial T(x,t)}{\partial t} = \alpha\frac{\partial^2 T(x,t)}{\partial x^2} \quad (2)$$

where α is thermal diffusivity.

3. Validation

Engine modelling still remains one of the most challenging topics for the automotive industry due to the amount of physical mechanisms involved and their inherent complexity. Therefore, the validation of the numerical results is a crucial step to ensure a set of solutions representative of the real in-cylinder processes. Hence, the main targets of this section are:

- To check the suitability of the kinetic mechanism used for the surrogate oxidation.
- To quantify the effects of H_2 addition in this mechanism.
- To validate the numerical model in real engine steady-state operation conditions.

3.1. Kinetic mechanism validation

The objective of this section is to check the suitability of the kinetic mechanism for reproducing both the flame speed and the auto-ignition delay of the fuel used for testing the engine, also with H_2 addition.

With this purpose, homogeneous reactor calculations with the selected chemical kinetic mechanism have been performed to obtain the laminar flame speed and the auto-ignition delay of different air/fuel mixtures. Then, the calculated results have been compared with

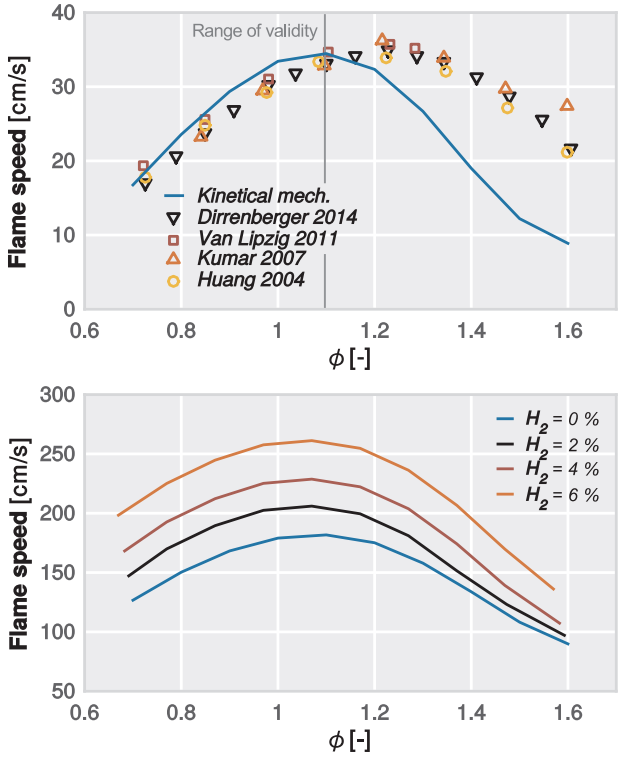

Fig. 4. Validation of the laminar flame speed of iso-octane/air mixture versus equivalence ratio at 298 K and 1 atm (top). Impact of H_2 addition on laminar flame speed at 1000 K, 10 atm and 10% of EGR (bottom).

experimental data available in the literature.

The plot at the top of Fig. 4 displays the comparison between the calculated laminar flame speeds of surrogate/air blends at ambient temperature (298 K) and standard pressure conditions (1 atm) and the measured data. For this comparison, no-dilution with either exhaust gas recirculation (EGR) or H_2 is used. The flame speed is plotted against the equivalence ratio in order to check the suitability of the kinetic mechanism to predict the trends of the experimental data available in the literature.

The results show that the flame speeds are well reproduced for low equivalence ratios ($\phi < 1.1$ or $\lambda > 0.9$), but the mechanism is not suitable for assessing rich iso-octane blends ($\phi > 1.1$ or $\lambda < 0.9$).

On the other side, Fig. 4 (bottom) shows results of a sensitivity study considering hydrogen addition. The objectives of this analysis are to evaluate the impact of H_2 addition on the laminar flame speed and also to determine the sensitivity of this additive in using the mechanism selected for this work. With this purpose, the flame speed has been calculated at 1000 K, 10 atm, 10% of EGR and two levels of H_2 concentration (0 and 6%).

As expected, results reveal that the flame speed increases when the hydrogen is mixed with the air/fuel mixture, following the same trends observed in the literature review.

An analogous study has been performed in order to validate the suitability of the kinetic mechanism to predict the auto-ignition delay in stoichiometric mixtures, so that could help to predict abnormal knocking combustion. In this case, the comparison with the experiments has been done at 50 bar without EGR. A wide sweep of mixture temperatures has been considered. Results plotted in Fig. 5 (top) show that the chosen mechanism reproduces quite well auto-ignition delays in the whole range of temperatures considered.

Fig. 5 (bottom) shows again a comparative analysis to evaluate the impact of H_2 addition on the ignition delay. In this case, the same conditions as in the previous graph were considered and an additional case with a 4% of H_2 was calculated. As can be seen, hydrogen addition

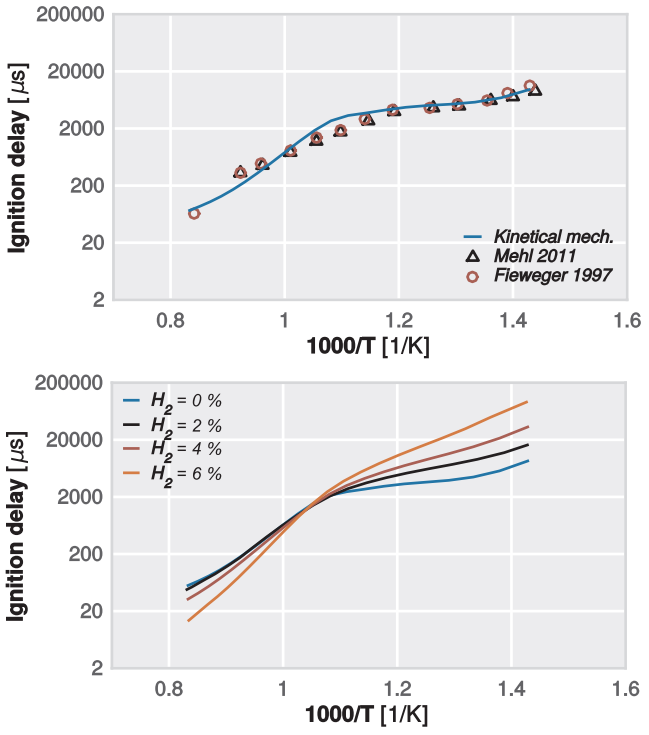

Fig. 5. Validation of the homogeneous ignition delay of stoichiometric iso-octane/air mixture versus temperature at 50 bar (top). Impact of H_2 addition on auto-ignition delay in stoichiometric iso-octane/air mixture at 50 bar (bottom).

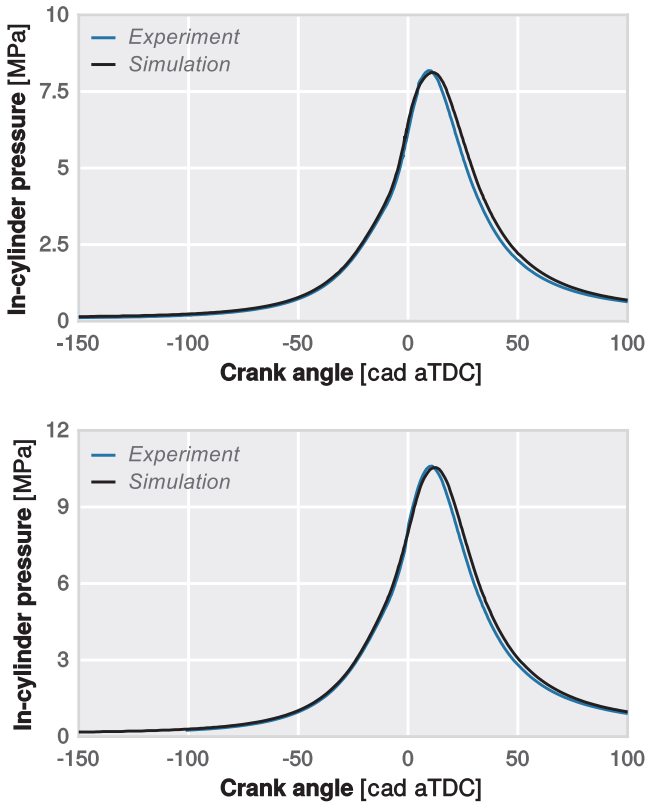

Fig. 6. Results of the model validation. Pressure traces are compared at 2500 rpm – 9 bar (top) and 3000 rpm – 13 bar (bottom).

helps to delay auto-ignition at lower temperatures but it reduces this delay as the temperature increases.

3.2. Model validation

The validation of the complete numerical model was performed for the uncoated engine and the two operation points described in Section 2. The measured data were obtained from tests with the real uncoated engine. Numerical results were validated by a direct comparison between calculated and measured in-cylinder pressure traces.

Fig. 6 shows the comparison in terms of pressure traces between simulations and measurements at the two conditions considered for the validation: 2500 rpm – 9 bar (#1) at the top, 3000 rpm – 13 bar (#2) at the bottom. In general, the calculations present a very good agreement with experiments for both operating points as is shown by the collapse of the numerical results with the measurements trace for almost the whole cycle in both cases. A slight difference can be observed only in the expansion stroke phase.

4. Results and discussion

In this section, the results obtained from the parametric study described in Section 2 are presented and discussed. First, a parametric study is performed considering a roughness sweep for the surfaces of both piston and cylinder head in the uncoated engine. Then, the same procedure was applied to the coated engine configuration in order to check if the presence of coating has some impact with respect to the previously observed trends. Finally, a comparison between the results with both engine configurations is discussed with the purpose of quantifying possible gains in terms of heat insulation and thermal efficiency.

4.1. Uncoated engine

In order to identify the effect of the surface roughness on the combustion, Fig. 7 shows the Rate of Heat Release (RoHR) obtained for the four different levels of surface roughness at both operation conditions considered. The difference between the smooth case and the rough ones is also displayed in the bottom plots of Fig. 7 to quantify the impact of the surface roughness on combustion.

Slight differences are appreciated with reasonable values of surface roughness (in the range between 0 and 14 μm). The peak value of the RoHR tends to decrease as the roughness rises at both operating conditions. Moreover, this parameter reach the lower values at 40 μm of surface roughness.

Since the observed differences can condition other engine outputs in a significant way, an analysis of the effect of roughness on both in-cylinder pressure and temperature is graphically shown in the plots of Fig. 8, respectively. In this case only Point #1 is included since both operation conditions show very similar trends.

Fig. 8 (top) shows that the maximum in-cylinder pressure decreases as the roughness increases. This trend can be explained by the burning rate lowering remarked in the Fig. 7. In addition, even not being showed in Fig. 8, the effect is slightly higher for the operating point at high speed and load. In-cylinder pressure is reduced as much as 1 bar at 2500 rpm – 9 bar, while the reduction at 3000 rpm – 13 bar is nearly 2.5 bar.

Similar comments can be remarked for the in-cylinder temperature evolution shown in the Fig. 8. The maximum value also decreases as the roughness is increased. Moreover, the impact is more evident at high engine speed/load (30 K versus 43 K).

Fig. 9 shows the heat transfer (HT) across the different surfaces of the chamber (piston, liner, cylinder head and total) for the four levels of roughness considered. As in Fig. 7, the percentage differences among the smooth-surfaces and the three rough-surfaces configurations are also plotted for getting a better quantification of the effects.

The results in Fig. 9 show that the impact trends are quite similar in both cases. HT decreases as the roughness is increased at both operation

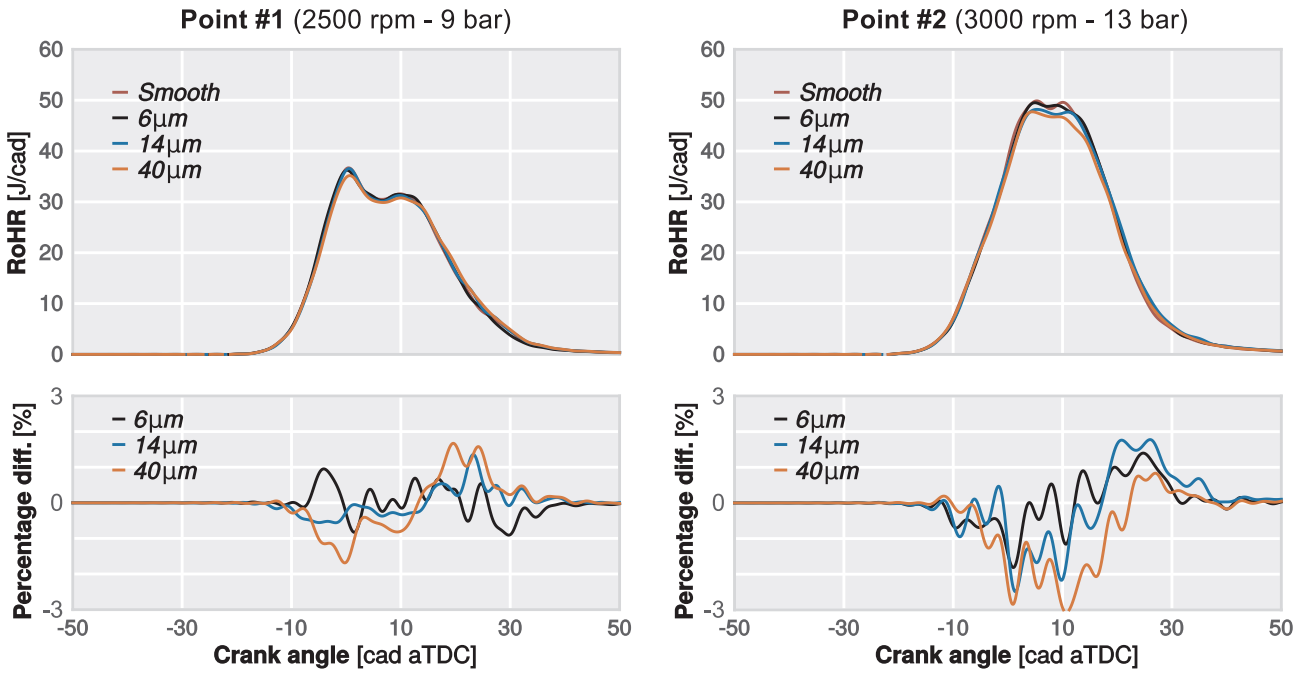

Fig. 7. Results of roughness study. RoHR traces are compared at 2500 rpm – 9 bar (left) and 3000 rpm – 13 bar (right) operating conditions. The percentage difference between the smooth case and the three other ones is also included at bottom.

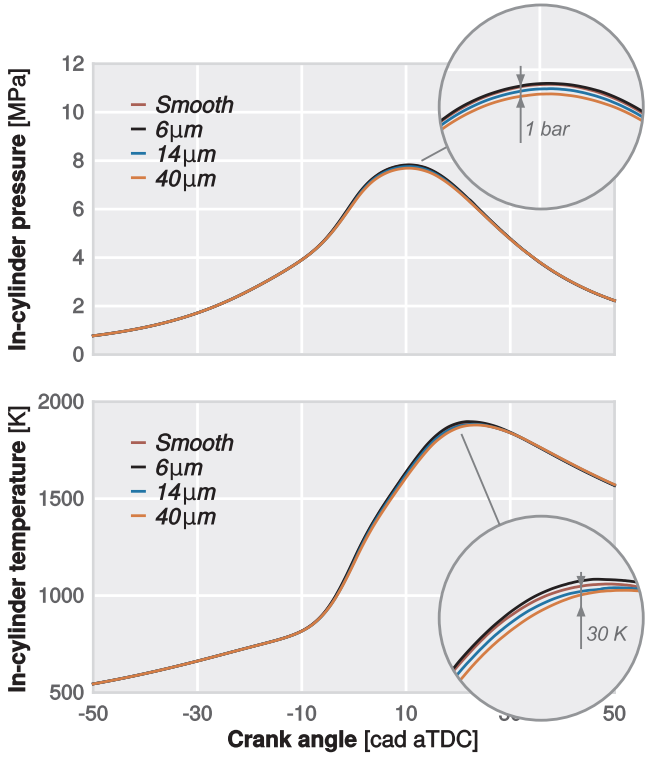

Fig. 8. Impact of roughness on pressure and temperature traces at 2500 rpm – 9 bar operating condition.

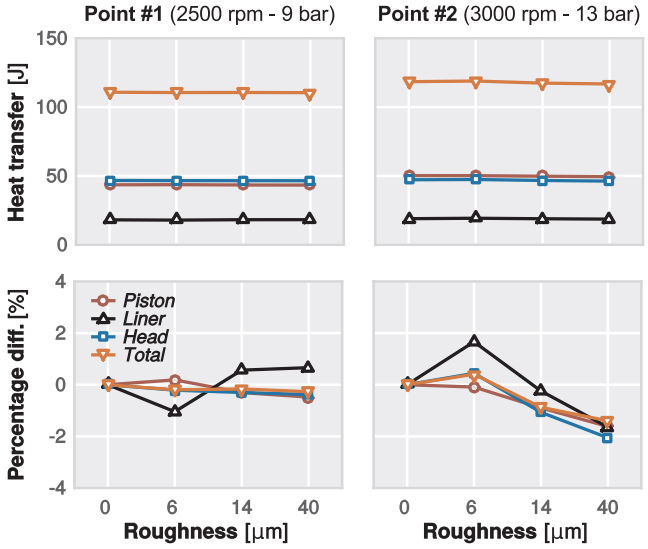

Fig. 9. Impact of roughness on heat transfer at 2500 rpm – 9 bar (left) and 3000 rpm – 13 bar (right) operating conditions. Percentage difference among the smooth case and the other three ones for both operating points is also included at bottom.

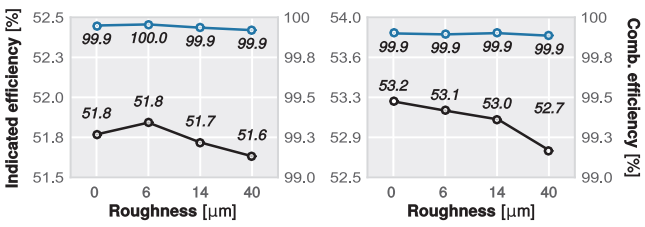

Fig. 10. Results of roughness study. Indicated efficiency trends are plotted at 2500 rpm – 9 bar (left) and 3000 rpm – 13 bar (right) operating conditions.

conditions. Nonetheless, significant variations of HT are only observed with the bigger roughness (14–40 μm) at high speed and load operation conditions. The current results would indicate that the HT differences should be principally due to the combustion variation.

Fig. 10 shows the impact trends of roughness on combustion and indicated efficiency at the two operation conditions considered. Results show that there is no effect of surface roughness on the combustion efficiency since its maximum does not exceed 0.1%. However, indicated

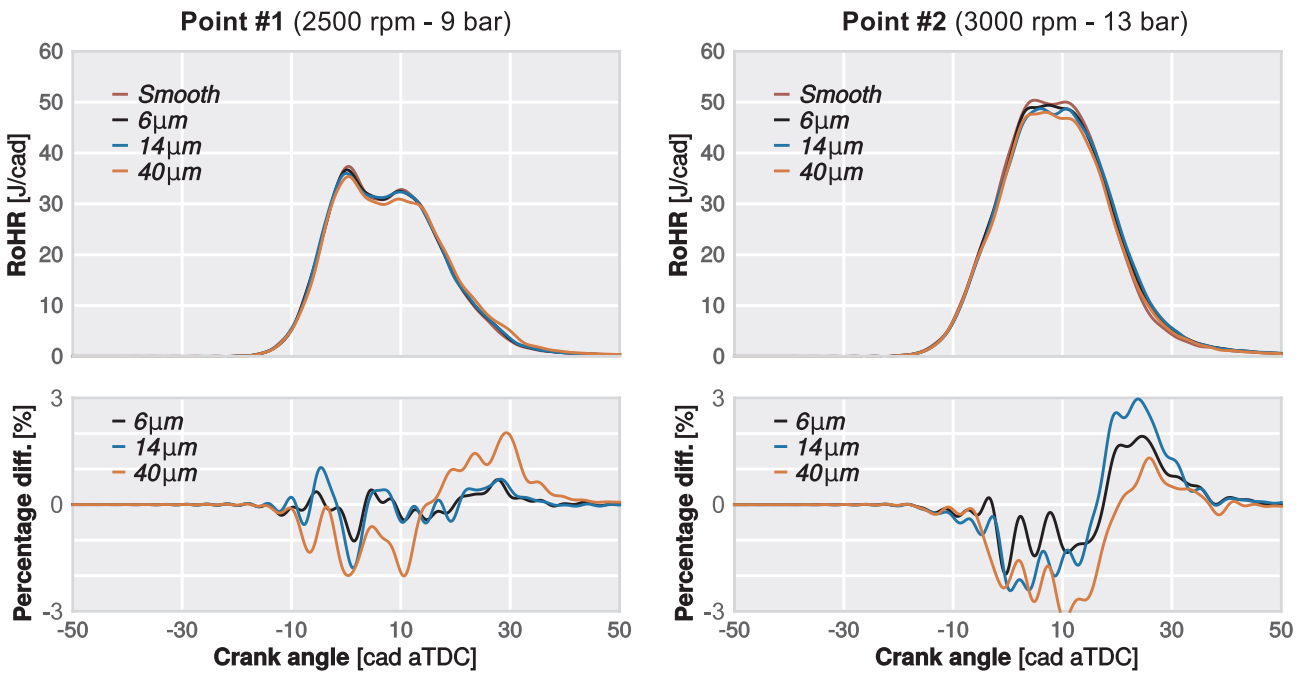

Fig. 11. Results of roughness study including coating layer. RoHR traces are compared at 2500 rpm – 9 bar (left) and 3000 rpm – 13 bar (right) operating conditions. The percentage difference between the smooth case and the three other ones is also included at bottom.

efficiency trends are somewhat correlated with those observed previously for the HT, they decrease when the surface roughness increases. This impact being more remarkable at the highest speed/load condition.

4.2. Coated engine

In this section, the results obtained with the same methodology as described in the previous section for the engine with coating insulation on the piston and cylinder head are discussed. The used coating material, for which the physical properties and thickness were displayed on Section 2, was considered in this analysis. To obtain the temperature evolution of the coated surfaces, the iterative process described in the same section linking the 1D HTM and CFD model was used. The results will be presented following the same scheme as in the prior uncoated engine study.

The profiles of the rate of heat release obtained for different wall roughness are plotted together and presented in Fig. 11.

As observed for the uncoated engine also, slight differences in RoHR are appreciated even with reasonable values of roughness (between 0 and 14 μm). The peak value of the energy release rate is also reduced as the roughness rises at both operating conditions and the differences are higher as the engine speed/load is increased. The burning rate increases at the end of the combustion as the roughness increases since the amount of unburned fuel is higher due to the lower burning velocities achieved in the previous combustion phase.

Wall roughness has a similar effect on the in-cylinder pressure as that previously observed for the energy release rate. Although for extension reasons it was deemed not to include the pressure and temperature profiles, it can be claimed from the results that the maximum pressure decreases due to the burning rate reduction caused by the roughness increase. In addition, the effect is clearly more apparent for the case at high speed and load in which the maximum pressure gap exceeds 3 bar, whereas in the lower speed/load case it reaches 2 bar at the most.

Similarly, as pointed out before about the impact of roughness on in-cylinder pressure trace, temperature profiles evidence that the maximum in-cylinder temperature is reduced as the surface roughness increases. This fact is probably also due to the reduction of combustion speed when roughness is increased. It is also observed that the maximum difference is larger for the higher speed and load condition (around 51 K) than for the lower speed/load case (almost 28 K). These differences are scarcely higher than those obtained for the uncoated engine.

Fig. 12 shows the HT across the different surfaces of the combustion chamber (piston, liner, cylinder head and total) calculated for the four levels of surface roughness considered in this study.

This figure shows that the heat rejection trends with increasing roughness are quite similar at both operating conditions. For the lower values of surface roughness, the total HT does not significantly change at any of the two engine running points. With the highest levels of

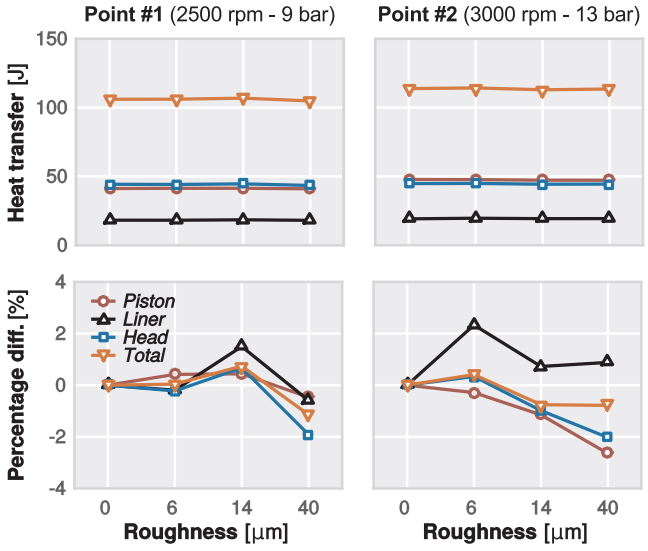

Fig. 12. Results of roughness study including coating layer. The impact of roughness on heat transfer at 2500 rpm – 9 bar (left) and 3000 rpm – 13 bar (right) operating conditions. Percentage difference among the smooth case and the other three ones for both operating points is also included at bottom.

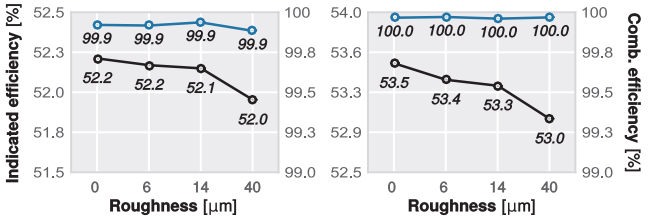

Fig. 13. Results of roughness study including coating layer. Indicated efficiency trends are plotted at 2500 rpm – 9 bar (left) and 3000 rpm – 13 bar (right) operating conditions.

roughness (> 14 μm) HT differences are remarkably higher and thereby, this could have a non-negligible impact on the thermal efficiency of the engine. Trends are slightly different to those obtained with the uncoated engine in which the HT decreases progressively with increasing surface roughness. Here significant differences can only be observed for the higher values of roughness (between 14 and 40 μm). It should be noted that HT increase in the liner is a consequence of the HT lowering through the cylinder head and piston. Since HT towards these latter surfaces is reduced, HT though the liner slightly increases.

Fig. 13 shows the impact trends of the indicated efficiency for the four surface roughness values. As obtained for the uncoated engine also, the roughness increase does not cause remarkable effects on the combustion efficiency. Again, the indicated efficiency trends are somewhat correlated with those obtained for the HT, the effect of the surface roughness being more significant at highest speed/load conditions.

4.3. Uncoated vs. coated engines

As a summary, in this final section a comparison between the results obtained for the uncoated and coated engines is presented. The target here is to quantify possible gain or loss in terms of both heat insulation and thermal efficiency that might be expected by isolating the surfaces of piston and cylinder head of a smoothed surfaces base-line engine (uncoated engine) with a 14 μm layer of the aforementioned coating material. This roughness value has been chosen because this corresponds to the peak value which is expected for the coatings developed for these particular applications.

The differences of the in-cylinder pressure traces for both operation conditions are shown in the plots of Fig. 14. These plots show that the effect of coated surfaces on the in-cylinder pressure trace is the opposite comparing both operation conditions. While the maximum pressure increases in the coated engine at 2500 rpm – 9 bar operation point, the maximum pressure is higher in the uncoated engine at 3000 rpm – 13 bar.

Fig. 15 shows the comparison of the RoHR traces in both engine configurations at the two operation conditions analysed. The second positive slope of the RoHR traces shown in these plots indicates that a tendency to knock may appear in both engine configurations. A visualisation of the flame propagation (based on the numerically obtained RoHR [46]) is included in the Fig. 15 in order to ensure that the second change of the RoHR slope is due to the end-gas auto-ignition rather than a speed up of the combustion. In addition, the knock tendency is quantified by the metric shown in Table 3. This metric is defined as the ratio between the RoHR maximum slopes achieved during the flame-propagated and knocking combustion. It can be seen, from Table 3, that this tendency increases with the coating layer at 2500 rpm – 9 bar, probably due to the reduction of the heat transfer at this condition. However, this trend seems not to be reproduced at higher engine speed/load since only a minor knocking is detected.

The differences of the burning rates observed during the second stage of the combustion due to the knock onset could explain the differences of the maximum pressure observed at the two operating points shown in Fig. 14. The higher burning rates obtained for the coated

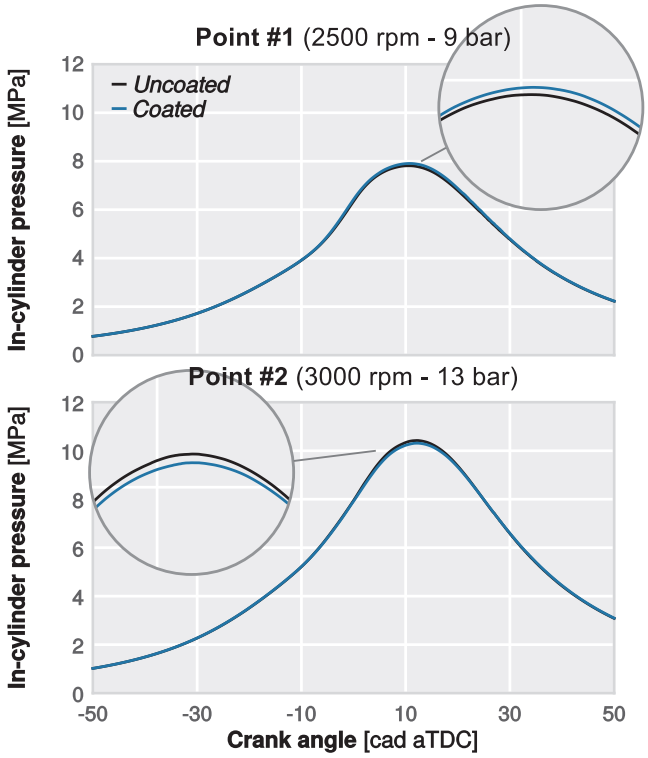

Fig. 14. Comparison between uncoated and coated engines. Pressure traces at 2500 rpm – 9 bar (top) and 3000 rpm – 13 bar (bottom) operating conditions.

engine might produce the higher in-cylinder pressure maximum at 2500 rpm – 9 bar. At 3000 rpm – 13 bar, the fuel burning rate for the uncoated engine is higher and consequently the maximum of in-cylinder pressure.

Finally, Table 4 show a comparison between uncoated and coated engines in terms of heat transfer trends, combustion and indicated efficiencies at 2500 rpm – 9 bar and 3000 rpm – 13 bar operating conditions. HT percentage difference between the uncoated engine and the coated for both operation points is also included. Results show that depending on the operation condition, gains between 3.59 and 4.67 % of heat loss reduction could be achieved with the coated version of the engine (isolating both piston and cylinder head with the reference coating material). This may lead to an improvement of the indicated efficiency of 0.3% and 0.1% at 2500 rpm – 9 bar and 3000 rpm – 13 bar, respectively.

5. Conclusions

This paper presents the calculations made to assess the effect of surface roughness on the combustion process on the one hand, and on the heat transfer to the walls of the engine on the other. A numerical methodology for understanding the mechanisms of heat transfer through the combustion chamber walls coated with advanced materials has been developed and validated. This tool has allowed quantifying the effects of the surface roughness on combustion and subsequently, on the heat transfer and thermal efficiency of the engine under study.

The main conclusions obtained from the uncoated engine simulations are:

- Some effect of the surface roughness on the combustion has been observed. The impact is more apparent with the highest roughness and at high speed/load operation.
- In general, the maximum rate of heat release is reduced as the roughness is increased.
- Similar trend as for RoHR has been observed for the total heat

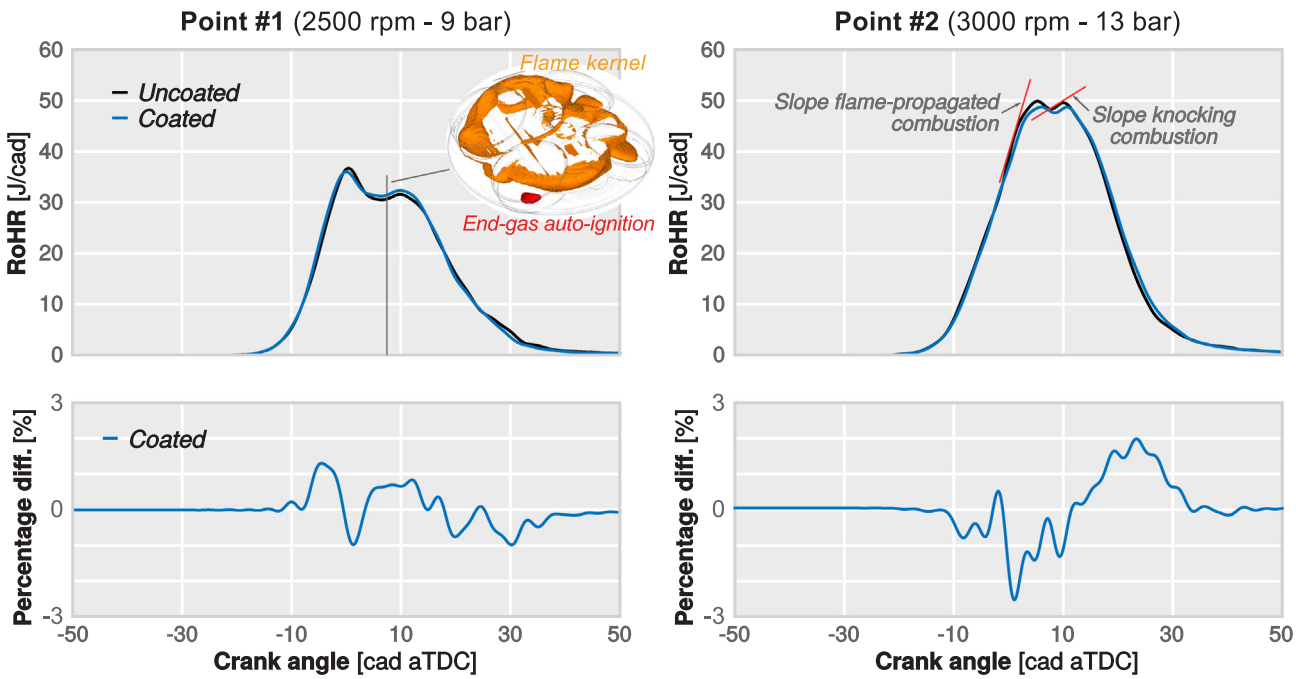

Fig. 15. Comparison between uncoated and coated engines. RoHR traces are compared at 2500 rpm – 9 bar (left) and 3000 rpm – 13 bar (right) operating conditions. The percentage difference between both cases for both operation points (bottom). Snapshot of the location of the end-gas auto-ignition at 2500 rpm – 9 bar (≈ 9 cad aTDC) is also included.

Table 3
Knock propensity of both engine configurations.

Operating point	Engine configuration	Knock intensity [%]
2500 rpm – 9 bar	Uncoated	77.8
2500 rpm – 9 bar	Coated	79.2
3000 rpm – 13 bar	Uncoated	53.6
3000 rpm – 13 bar	Coated	47.1

transfer in the combustion chamber.

- Considering that the roughness has not impact on the convective heat transfer coefficient, the results obtained with closed cycle calculations seem to indicate that the heat transfer variation is mainly due to variations in the combustion process.
- There is no gain in terms of HT for realistic values of surface roughness (14 μm) for the lower engine speed/load operation condition whereas a small gain of 1% is achieved at higher speed/load conditions.

The results of the coated engine calculations showed that:

- No remarkable differences on heat transfer below 14 μm of roughness are obtained.
- Again, it is observed that HT has not changed for realistic values of surface roughness (14 μm) for the lower engine speed/load operation condition while a gain of 1% is achieved at higher speed/load conditions.
- Despite this improvement, the indicated efficiency is reduced by 0.2%.

Finally, the comparison between the uncoated and coated engines has shown that:

- Maximum gains of 3.59–4.67% in heat loss could be achieved by covering the piston and cylinder head with a 14 μm layer of the coating material.
- Considering that the effect of the surface roughness is negligible at low speed/load conditions and almost 1% for the high speed/load ones, similar gains in HT are observed (3.58 versus 3.67%) in both operating points.
- This fact could allow getting an indicated efficiency improvement of 0.1–0.3%, but the risk of knock increases at medium load/speed operation. Nonetheless, combined with other well-known strategies for mitigating knock such as ultra-lean combustion and/or increased boosting, smart coatings may slightly contribute to the search for higher levels of efficiency in SI engines.

Acknowledgements

This project has received funding from the European Union's Horizon 2020 research and innovation programme under grant agreement No. 724084.

J. Gomez-Soriano is partially supported through the Programa de Apoyo para la Investigación y Desarrollo (PAID) of Universitat

Table 4
Comparison between uncoated and coated engines in terms of heat transfer trends, combustion and indicated efficiencies at 2500 rpm – 9 bar and 3000 rpm – 13 bar operating conditions.

Operating point	Engine configuration	Heat transfer [J]	HT perc. diff. [%]	Comb. eff. [%]	Ind. eff. [%]
2500 rpm – 9 bar	Uncoated smooth	110.82	–	99.90	51.77
2500 rpm – 9 bar	Coated 14 μm	106.84	−3.59	99.94	52.13
3000 rpm – 13 bar	Uncoated smooth	118.48	–	99.95	53.2
3000 rpm – 13 bar	Coated 14 μm	112.95	−4.67	99.96	53.3

Politècnica de València [Grant No. FPI-S2-2016-1353].

The authors want to express their gratitude to CONVERGENT SCIENCE Inc. and Convergent Science GmbH for their kind support for the CFD calculations with the CONVERGE software.

References

[1] Z. Wang, H. Liu, R.D. Reitz, Knocking combustion in spark-ignition engines, Prog. Energy Combust. Sci. 61 (Supplement C) (2017) 78–112, https://doi.org/10.1016/j.pecs.2017.03.004.

[2] D. Bradley, 'Hot spots' and gasoline engine knockJournal of the Chemical Society, J. Chem. Soc. Faraday Trans. 92 (16) (1996) 2959–2964, https://doi.org/10.1039/FT9969202959.

[3] P. Aleiferis, Y. Hardalupas, A. Taylor, K. Ishii, Y. Urata, Flame chemiluminescence studies of cyclic combustion variations and air-to-fuel ratio of the reacting mixture in a lean-burn stratified-charge spark-ignition engine, Combust. Flame 136 (1–2) (2004) 72–90.

[4] M. Riess, A. Benz, M. Wöbke, M. Sens, Einlassseitige ventilhubstrategien zur turbulenzgenerierung, MTZ-Motortechnische Zeitschrift 74 (7-8) (2013) 580–585.

[5] M. Sens, S. Zwahr, M. Günther, Potenziale des variablen verdichtungsverhältnisses am voll gemillerten ottomotor, MTZ-Motortechnische Zeitschrift 77 (4) (2016) 52–58.

[6] B. Sendyka, M. Cygnar, Stratified charge combustion in a spark-ignition engine with direct injection system, Advances in Internal Combustion Engines and Fuel Technologies, InTech, 2013.

[7] M.B. Young, Cyclic dispersion in the homogeneous-charge spark-ignition engine - a literature survey, in: SAE International Congress and Exposition. doi:https://doi.org/10.4271/810020.

[8] J. Pan, N. Li, H. Wei, J. Hua, G. Shu, Experimental investigations on combustion acceleration behavior of methane/gasoline under partial load conditions of si engines, Appl. Therm. Eng. 139 (2018) 432–444, https://doi.org/10.1016/j.applthermaleng.2018.04.123.

[9] S. Shrestha, G. Karim, Hydrogen as an additive to methane for spark ignition engine applications, Int. J. Hydrogen Energy 24 (6) (1999) 577–586, https://doi.org/10.1016/S0360-3199(98)00103-7.

[10] X. Yu, H. Wu, Y. Du, Y. Tang, L. Liu, R. Niu, Research on cycle-by-cycle variations of an si engine with hydrogen direct injection under lean burn conditions, Appl. Therm. Eng. 109 (2016) 569–581, https://doi.org/10.1016/j.applthermaleng.2016.08.077.

[11] M. Wu, Y. Pei, J. Qin, X. Li, J. Zhou, Z.S. Zhan, Q.-y. Guo, B. Liu, T.G. Hu, Study on methods of coupling numerical simulation of conjugate heat transfer and in-cylinder combustion process in GDI engine, in: WCX™17: SAE World Congress Experience. doi:https://doi.org/10.4271/2017-01-0576.

[12] F. Berni, G. Cicalese, S. Fontanesi, A modified thermal wall function for the estimation of gas-to-wall heat fluxes in CFD in-cylinder simulations of high performance spark-ignition engines, Appl. Therm. Eng. 115 (2017) 1045–1062, https://doi.org/10.1016/j.applthermaleng.2017.01.055.

[13] L. Zhang, Parallel simulation of engine in-cylinder processes with conjugate heat transfer modeling, Appl. Therm. Eng. 142 (2018) 232–240, https://doi.org/10.1016/j.applthermaleng.2018.06.084.

[14] P. Kundu, R. Scarcelli, S. Som, A. Ickes, Y. Wang, J. Kiedaisch, M. Rajkumar, Modeling heat loss through pistons and effect of thermal boundary coatings in diesel engine simulations using a conjugate heat transfer model. doi:https://doi.org/10.4271/2016-01-2235.

[15] C.D. Rakopoulos, D.C. Rakopoulos, G.C. Mavropoulos, E.G. Giakoumis, Experimental and theoretical study of the short term response temperature transients in the cylinder walls of a diesel engine at various operating conditions, Appl. Therm. Eng. 24 (5) (2004) 679–702, https://doi.org/10.1016/j.applthermaleng.2003.11.002.

[16] K. Fukui, Y. Wakisaka, K. Nishikawa, Y. Hattori, H. Kosaka, A. Kawaguchi, Development of instantaneous temperature measurement technique for combustion chamber surface and verification of temperature swing concept, in: SAE 2016 World Congress and Exhibition. doi:https://doi.org/10.4271/2016-01-0675.

[17] H. Kosaka, Y. Wakisaka, Y. Nomura, Y. Hotta, M. Koike, K. Nakakita, A. Kawaguchi, Concept of "temperature swing heat insulation in combustion chamber walls, and appropriate thermo-physical properties for heat insulation coat, SAE Int. J. Engines 6 (1) (2013) 142–149, https://doi.org/10.4271/2013-01-0274.

[18] Y. Wakisaka, M. Inayoshi, K. Fukui, H. Kosaka, Y. Hotta, A. Kawaguchi, N. Takada, Reduction of heat loss and improvement of thermal efficiency by application of "temperature swing insulation to direct-injection diesel engines, SAE Int. J. Engines 9 (3) (2016) 1449–1459, https://doi.org/10.4271/2016-01-0661.

[19] T. Kogo, Y. Hamamura, K. Nakatani, T. Toda, et al., High efficiency diesel engine with low heat loss combustion concept - Toyota's inline 4-cylinder 2.8-liter ESTEC 1GD-FTV Engine, SAE Technical Paper 2016-01-0658, 2016, https://doi.org/10.4271/2016-01-0658.

[20] J. Kashdan, G. Bruneaux, Laser-induced phosphorescence measurements of combustion chamber surface temperature on a single-cylinder diesel engine, SAE Technical Paper 2011-01-2049, 2011, https://doi.org/10.4271/2011-01-2049.

[21] M. Algotsson, C. Knappe, M. Tunér, M. Richter, B. Johansson, M. Aldén, In-cylinder surface thermometry using laser induced phosphorescence, 2012, pp. 482–487. Copyright 2012 by the Japan Society of Mechanical Engineers.

[22] J.B. Heywood, Internal Combustion Engine Fundamentals, McGraw-Hill Inc, 1998.

[23] C. Rakopoulos, G. Mavropoulos, D. Hountalas, Measurements and analysis of load and speed effects on the instantaneous wall heat fluxes in a direct injection air-cooled diesel engine, Int. J. Energy Res. 24 (7) (2000) 587–604.

[24] J. Chang, O. Güralp, Z. Filipi, D. Assanis, et al., New heat transfer correlation for an HCCI engine derived from measurements of instantaneous surface heat flux, SAE Technical Paper 2004-01-2996, 2004, https://doi.org/10.4271/2004-01-2996.

[25] A. Kikusato, K. Terahata, K. Jin, Y. Daisho, A numerical simulation study on improving the thermal efficiency of a spark ignited engine—part 2: Predicting instantaneous combustion chamber wall temperatures, heat losses and knock—, SAE Int. J. Engines 7 (1) (2014) 87–95.

[26] Convergent Science Inc., Converge 2.3 Theory Manual, 2018.

[27] V. Yakhot, S. Orszag, Renormalization group analysis of turbulence, J. Sci. Comput. 1 (1) (1986) 3–51, https://doi.org/10.1007/BF01061452.

[28] A.A. Amsden, P.J. O'rourke, T.D. Butler, KIVA-II: A computer program for chemically reactive flows with sprays, Tech. rep., Los Alamos National Laboratory, NM USA, 1989.

[29] O. Redlich, J.N.S. Kwong, On the thermodynamics of solutions. V. An equation of state. fugacities of gaseous solutions, Chem. Rev. 44 (1) (1949) 233–244, https://doi.org/10.1021/cr60137a013.

[30] R.I. Issa, Solution of the implicitly discretised fluid flow equations by operator-splitting, J. Comput. Phys. 62 (1986) 40–65, https://doi.org/10.1016/0021-9991(86)90099-9.

[31] S.D. Givler, M. Raju, E. Pomraning, P.K. Senecal, N. Salman, R. Reese, Gasoline combustion modeling of direct and port-fuel injected engines using a reduced chemical mechanism, in: SAE 2013 World Congress & Exhibition. doi:https://doi.org/10.4271/2013-01-1098.

[32] E. Pomraning, K. Richards, P.K. Senecal, Modeling turbulent combustion using a rans model, detailed chemistry, and adaptive mesh refinement, in: SAE 2014 World Congress & Exhibition. doi:https://doi.org/10.4271/2014-01-1116.

[33] R. Scarcelli, K. Richards, E. Pomraning, P.K. Senecal, T. Wallner, J. Sevik, Cycle-to-cycle variations in multi-cycle engine RANS simulations, in: SAE 2016 World Congress and Exhibition. doi:https://doi.org/10.4271/2016-01-0593.

[34] A. Robert, S. Richard, O. Colin, T. Poinsot, Les study of deflagration to detonation mechanisms in a downsized spark ignition engine, Combust. Flame 162 (7) (2015) 2788–2807, https://doi.org/10.1016/j.combustflame.2015.04.010.

[35] A. Robert, S. Richard, O. Colin, L. Martinez, L.D. Francqueville, Les prediction and analysis of knocking combustion in a spark ignition engine, Proc. Combust. Inst. 35 (3) (2015) 2941–2948, https://doi.org/10.1016/j.proci.2014.05.154.

[36] P.K. Senecal, E. Pomraning, K.J. Richards, T.E. Briggs, C.Y. Choi, R.M. McDavid, M. A. Patterson, Multi-dimensional modeling of direct-injection diesel spray liquid length and flame lift-off length using CFD and parallel detailed chemistry, SAE Technical Paper 2003-01-1043. doi:https://doi.org/10.4271/2003-01-1043.

[37] A. Babajimopoulos, D.N. Assanis, D.L. Flowers, S.M. Aceves, R.P. Hessel, A fully coupled computational fluid dynamics and multi-zone model with detailed chemical kinetics for the simulation of premixed charge compression ignition engines, Int. J. Engine Res. 6 (5) (2005) 497–512, https://doi.org/10.1243/146808705X30503.

[38] P. Pal, D. Probst, Y. Pei, Y. Zhang, M. Traver, D. Cleary, S. Som, Numerical investigation of a gasoline-like fuel in a heavy-duty compression ignition engine using global sensitivity analysis, SAE Int. J. Fuels Lubr. 10 (1) (2017) 56–68, https://doi.org/10.4271/2017-01-0578.

[39] P. Pal, Computational Modeling and Analysis of Low Temperature Combustion Regimes for Advanced Engine Applications (Ph.D. thesis), University of Michigan-Ann Arbor, 2016.

[40] R. Scarcelli, N. Matthias, T. Wallner, Numerical investigation of combustion in a lean burn gasoline engine, in: 11th International Conference on Engines & Vehicles. doi:https://doi.org/10.4271/2013-24-0029.

[41] H. Wang, M. Yao, R.D. Reitz, Development of a reduced primary reference fuel mechanism for internal combustion engine combustion simulations, Energy Fuels 27 (12) (2013) 7843–7853, https://doi.org/10.1021/ef401992e.

[42] X. Yang, A. Solomon, T.-W. Kuo, Ignition and combustion simulations of spray-guided sidi engine using arrhenius combustion with spark-energy deposition model, in: SAE 2012 World Congress & Exhibition. doi:https://doi.org/10.4271/2012-01-0147.

[43] A.J. Torregrosa, P. Olmeda, B. Degraeuwe, M. Reyes, A concise wall temperature model for DI Diesel engines, App. Therm. Eng. 26 (11–12). doi:https://doi.org/10.1016/j.applthermaleng.2005.10.021.

[44] T. Cebeci, J. Cousteix, Modeling and computation of boundary-layer flows–solutions manual and computer programs, Book Rev. 22 (2003) 199–202.

[45] Adrian Bejan, Allan D. Kraus, Heat Transfer Handbook, Vol. 1, John Wiley & Sons, 2003.

[46] Stephane Chevillard, et al., Advanced methodology to investigate knock for downsized gasoline direct injection engine using 3D RANS simulations, No. 2017-01-0579, SAE Technical Paper, 2017.